energy&fuels

Article

Thermal cracking of oil under water pressure up to 900 bar at high thermal maturities 1. Gas compositions and carbon isotopes

Liujuan Xie, Yongge Sun, Clement N. Uguna, Youchuan Li, Colin E. Snape, and Will Meredith

Energy Fuels, **Just Accepted Manuscript** • DOI: 10.1021/acs.energyfuels.5b02792 • Publication Date (Web): 04 Mar 2016

ACS Publications

Energy & Fuels is published by the American Chemical Society. 1155 Sixteenth Street N.W., Washington, DC 20036

Thermal cracking of oil under water pressure up to 900 bar at high thermal maturities 1. Gas compositions and carbon isotopes

Liujuan Xie[1, 2], Yongge Sun[1*], Clement N. Uguna[3, 5], Youchuan Li[4], Colin E. Snape[3], Will Meredith[3]

[1] Department of Earth Science, Zhejiang University, Hangzhou 310027, China.

[2] Research Institute of Unconventional Petroleum and Renewable Energy, China University of Petroleum, Qingdao 266580, China.

[3]Faculty of Engineering, University of Nottingham, Energy Technologies Building, Triumph Road, Nottingham NG7 2TU, UK.

[4] Beijing Research Center of CNOOC China Ltd., Beijing 100027, China.

[5] Centre for Environmental Geochemistry, British Geological Survey, Keyworth, Nottingham, NG12 5GG, UK.

*Corresponding author. ygsun@zju.edu.cn (Y. Sun).

Abstract

In this study, a C_9^+ fraction of saturate-rich Tertiary source rock-derived oil from the South China Sea basin was pyrolysed in normal and supercritical water using a 25 mL vessel at a range of temperature from 350 to 425 °C for 24 h, to probe pressure effects up to 900 bar on gas yields and their stable carbon isotopic compositions during thermal cracking. Pressure generally retards oil cracking, as evidenced by

reduced gas yields, but the trends depend upon the level of thermal evolution. In the early stages of cracking (350 and 373 °C, equivalent vitrinite reflectance of < ~1.1% R_o), the suppression effect increases with pressure from 200 to 900 bar but it is most marked between 200 and 470 bar. At the later stages in the wet gas window (390, 405 and 425 °C, equivalent vitrinite reflectance of > 1.3% R_o), pressure still has a strong suppression effect from 200 to 470 bar, which then levels off or is reversed as the pressure is increased further to 750 and 900 bar. Interestingly, the stable carbon isotopic composition of the generated methane becomes enriched in ^{13}C as the pressure increases from 200 to 900 bar. A maximum fractionation effect of ~3‰ is observed over this pressure range. Due to pressure retardation, the isotopically heaviest methane signature does not coincide with the maximum gas yield, contrary to what might be expected. In contrast, pressure has little effect on ethane, propane and butane carbon isotope ratios, which show maximum variation of ~1‰. The results suggest that the rates of methane-forming reactions affected by pressure control methane carbon isotope fractionation. Based on distinctive carbon isotope patterns of methane and wet gases from pressurized oil cracking, a conceptual model using "natural gas plot" is constructed to identify pressure effect on *in-situ* oil cracking providing other factors excluded. The transition in going from dry conditions to normal and supercritical water does not have a significant effect on oil-cracking reactions as evidenced by gold bag hydrous and anhydrous pyrolysis results at the same temperatures as used in the pressure vessel.

Keywords: Oil cracking; high water pressure; hydrous pyrolysis; supercritical conditions; pressure retardation; carbon stable isotopes.

1. Introduction

Due to increasing interest in exploration for deeply buried oil/gas reservoirs in petroliferous basins around the world, much attention has focused on evaluating the thermal stability of crude oil under high temperature-pressure conditions. Classical petroleum generation theory contends that temperature is the principal variable in hydrocarbon generation and destruction and that pressure can be ignored or is comparatively less important.[1, 2] Using this hypothesis, kinetic models of petroleum generation and destruction were developed to predict the maximum temperature or depth at which oil can be discovered. However, the discovery of liquid hydrocarbons in deeply buried source or reservoir rocks beyond the degradation window of crude oil suggests that factors other than temperature influence the thermal stability of crude oil under high temperature/high pressure (HT/HP) conditions.[3, 4] Pressure has been considered to be an important candidate to account for these observations.[5-7]

Many laboratory studies have been performed to better understand pressure effects on organic matter maturation, hydrocarbon generation and destruction. However, much of this work has resulted in conflicting conclusions (e.g., Carr[8] and Mi et al.[9], and references therein). The main points can be summarized here based on previous studies on pressure effects on kerogen or coal: (i) negligible effects;[10-12] (ii) significant suppression;[7, 13-16] (iii) promotion effects.[17-19] Goodarzi[20] claimed that the effect of pressure varies depending on the range of temperatures and pressures, as also observed by Behar and Vandenbroucke.[21] Price and Wenger[13] noted that the pressure effect is not continuous with certain threshold pressures (variable with temperature) needing to be reached before the effect becomes significant. Carr[8] concluded that the differences in interpretation could be due to lack of fundamental understanding of the pressure effect on maturation and hydrocarbon generation. Carr et al.[22] suggested that

chemical reactions associated with hydrocarbon generation and maturation could be endothermic volume expansion reactions, which are controlled by both the system pressure and temperature. Recent work by Mi et al.[9] indicated that the previously conflicting results may be caused by the different pressure ranges under which the experiments were conducted.

Also a number of studies on cracking of crude oils[12, 23-25] and model compounds[21, 26-28] have measured gas yields, stable carbon isotopic fractionation and kinetics during the cracking process, and some of these investigated pressure effects on oil cracking. Dominé[27] showed that the rates and products of pure hydrocarbon pyrolysis were hindered by increasing pressure over the range of 210–15600 bar and 290–365 °C. Jackson et al.[29] suggested that pressure retards *n*-hexadecane cracking at 150–600 bar and 300–370 °C. However, sealed gold-tube experiments of model compounds at 325–430°C showed that pressure accelerates cracking rates when the pressure is lower than ~400 bar, while retardation was observed above 400 bar.[21, 30] Transition state theory, in which reaction rates of oil/model compounds are controlled by the activation volume, was introduced to explain the promotion-suppression phenomenon.[21, 26, 30] Hill et al.[31] investigated the effect of pressure on crude oil cracking at 350–400 °C. Cracking rates were enhanced slightly at pressures up to ~600–700 bar compared to 90 bar, followed by retardation when experimental pressures were >600–700 bar.

In summary, the effect of pressure on the thermal stability of crude oil still remains speculative. The published contradictory results may be due to the variety of laboratory conditions and different samples, e.g., pyrolysis temperature, pressure range, hydrous or anhydrous pyrolysis, sample types. Taking pressure vessels for example, the majority of pyrolysis experiments described in the literature used

flexible gold bags or gold tubes (confined conditions). In high pressure confined pyrolysis, the pressure is applied externally on the wall of the gold bags/tubes. The gaseous products cause a volume increase during pyrolysis, leading to the gold bags/tubes swelling to maintain constant internal pressure with the creation of additional vapor space.

In this study, a pressurized vessel used by Carr et al.[22] and Uguna et al.[15, 16, 32] was adopted. The pressure is derived by volume expansion of the water inside the fixed volume vessel. Additional water is added to the vessel to achieve the required pressure at the start of each experiment. Carr et al.[22] pyrolysed Kimmeridge Clay at temperatures between 310 and 350 °C and water pressure up to 500 bar. They found that bitumen and gas generation were retarded at 500 bar. Similarly, Uguna et al.[32] studied two high-volatile coals at pyrolysis temperatures of 350 °C. The results showed that gas yields are proportionally reduced more than bitumen yields with increasing water pressure up to 900 bar. In our pyrolysis vessel, the water acts as pressurizing phase that is in direct contact with the sample. The vessel is entirely filled with water and sample at the reaction temperature, thereby leaving little or no space for gaseous products, which results in retarded reactions as described in previous work.[15, 16, 22, 32] Therefore, water pressure pyrolysis experiments may provide a more comprehensive understanding of the effect of pressure on petroleum generation. Similar high pressure hydrous pyrolysis studies also observed the retardation effect of pressure on hydrocarbon generation and maturation, and indicated that water is an important factor.[13, 33]

Using a C_9^+ fraction of saturate-rich oil derived from Tertiary source rock in the South China Sea, hydrous, fixed-volume pressure vessel pyrolysis experiments were conducted under low and high water-pressure conditions. This study aims to

investigate the magnitude of enhancement or suppression of oil cracking rates based on the gas generated with increasing pressure at different thermal stages, and probe potential pressure effects on oil cracking by gas isotope geochemistry. It is the first to investigate oil cracking at high thermal maturities under high pressure liquid water and also to report the effects of pressure on both gas yields and stable carbon isotope ratios. Oil compositions and compound-specific carbon isotopes will be addressed in a subsequent publication.

2. Sample and experimental

2.1 Sample

The crude oil used in this study was collected from the Pearl River Mouth Basin (Zhujiangkou Basin), South China Sea. The oil composition in terms of saturates, aromatics, resins and asphaltenes (SARA) and carbon isotopic values are presented in Figure 1. It is saturate-rich oil with 22° API gravity and 0.14% sulfur content. The stable carbon isotope values of original oil, saturates, aromatics, resins and asphaltenes are -27.0‰, -27.5‰, -26.8‰, -26.0‰ and -26.4‰, respectively. As shown in the whole oil gas chromatogram, light hydrocarbons ($<C_8$) in the oil are low, which might result from slight biodegradation (as indicated by a prominent unresolved complex mixture as UCM on the chromatogram) and natural volatilization of crude oil during sample collection, transportation and storage.

2.2 High water-pressure pyrolysis experiments

The hydrothermal pyrolysis equipment comprised a 25 mL Hastelloy cylindrical pressure vessel rated to 1400 bar at 420 °C connected to a pressure gauge and rupture disc rated to 950 bar (Figure 2). The experiments were conducted using 1.20 g of

crude oil at five different temperatures, each for 24 h duration under low pressure hydrous (200 bar) and high pressure (470, 750 and 900 bar) pyrolysis conditions, as described in detail in Uguna et al.[16] In order to relate the experimental pressures employed to those which occur in real geological basins, here follows a brief description on crustal geostatic gradients. Although the depth of the oil and gas windows may vary due to differing geothermal gradients (assume ~25 °C/km), and kinetics of the kerogen in the source rock, we can assume top of the oil and gas window occurs at 3 and 4 km, respectively. Based on usually applied rock mass of 2.5 $\times$ 10^3 kg/m^3 and gravitational acceleration of 9.8 m/s^2, we might expect pressures near 735 and 980 bars at 3 and 4 km, respectively. Therefore, the high pressures in our experiments might be similar to those in natural conditions. Of course, this calculation does not consider overpressure caused by compaction disequilibrium or petroleum generation, nor does it consider the upper limit of overpressure, i.e., the fracture gradient.

Temperatures were set at 350, 373, 390, 405, and 425 °C (accuracy ±1 °C). According to the Lewan's definition[34], the hydrothermal experiments carried out with temperatures 350 and 373 °C under the set pressure are defined as hydrous pyrolysis, although the pressure vessel is filled with liquid water leaving no vapour space to best simulate the deep sub-surface. At 390, 405 and 425 °C, hydrothermal pyrolysis is in the supercritical water provided the pressure is higher than the supercritical pressure of 221 bar. In order to clarify whether there are any effects associated with the transition from dry conditions to liquid and supercritical water, parallel hydrous and anhydrous gold tube pyrolysis with fixed pressure of 450 bar for 24 h at temperatures of 370, 390 and 405 °C were carried out. Details of the apparatus employed and experimental procedure used in the gold tube pyrolysis experiments are the same as

described in previous work[28] then are not summarized here. The equivalent vitrinite reflectance at different temperatures was calculated using the Easy%R_o kinetic model.[35] As listed in Table 1, the calculated vitrinite reflectance of the set temperatures are 0.92, 1.15, 1.35, 1.56, 1.85 %R_o, respectively. Therefore, the thermal maturity reached during the experiments covers the peak oil generation stage to an elevated stage in the wet gas window.

The oil was weighed, transferred to the vessel, and then the deoxygenated and distilled water (~10 mL) was added to result in a pressure close to 200 bar at 350 and 373 °C. Note the observed pressure is less than the actual pressure due to the temperature gradient existing between the not reaction vessel and the gauge. However, including the dead volume, the filing factor water with 10 ml of water is higher than the supercritical density of water meaning that the supercritical state should be achieved at 374 °C and higher temperatures. The reactor vessel was flushed with nitrogen gas to replace the air in the vessel head space, after which 2 bar pressure of nitrogen was pumped into the vessel to produce an inert atmosphere during the pyrolysis runs. A sand bath connected to a constant flow of compressed air source was pre-heated to the setting temperature and left to equilibrate. The sand bath was lifted using a jack to enclose the vessel and left to run for 24 h. The temperature of the vessel was also monitored independently by means of a K-Type thermocouple attached to the outside of the vessel and recorded by computer every 10 seconds.

The high liquid water pressure (470, 750 and 900 bar) experiments were performed using a procedure similar to the lower pressure tests (200 bar), with the vessel initially filled with 20 mL deoxygenated water. After lowering the pressure vessel into the sand bath, the vessel was connected to the high liquid-water pressure

line and allowed to attain its maximum pressure of 175 bar (in about 30 min) before the addition of more water to increase the pressure. This procedure is employed to prevent too much water being added to the vessel, which might lead to generation of overpressure in excess of the pressure limit of the system. To apply high water pressure to the system with the aid of a compressed air driven liquid pump, the emergency pressure release valve B was first closed (Figure 2), and valve A was opened until a pressure slightly higher than the pressure of the experiment was displayed on the external pressure gauge. This avoided losing any content of the vessel when reactor valve C was opened. High liquid-water pressure was then applied to the system by first opening valve C and immediately gradually opening valve A to add more distilled water into the reaction vessel. Although likely to have an effect, pH was kept neutral to avoid corrosion of the vessel. When the required pressure was attained, valve C was closed to isolate the reactor from the high water-pressure line, and valve A was also closed to prevent more water from entering the pressure line. Valve B was opened to vent the excess pressure on the line. The experiment was then allowed to run (leaving valve C tightly closed to avoid losing generated products) for the required time, after which the sand bath was switched off and left to cool to ambient temperature before product recovery.

2.3 Chemical and isotopic analyses of gas components

After the pyrolysis experiment, the high water-pressure line was disconnected and a connector was attached to valve C. The generated gas was collected and transferred to a gas bag with the aid of a gas tight syringe via the connector by opening valve C.

Gas analysis was performed using a Clarus 580 gas chromatograph (GC) fitted with FID and TCD detectors operating at 200 °C. The GC was equipped with an

alumina plot fused silica capillary column (30 m × 0.32 mm × 10 μm) and helium was the carrier gas. Gas samples (100 μl) were injected with the split ratio 10:1 at 100 °C. The temperature was kept constant at 60 °C (13 min hold), then increased to 180 °C (10 min hold) at 10 °C/min. Individual hydrocarbon gas yields, H_2 and CO_2 gas yields were determined quantitatively in relation to methane, H_2 and CO_2 (injected separately) as external gas standards, respectively. The total yield of generated hydrocarbon gases was calculated using the total volume of generated gas collected in relation to the aliquot volume of gas introduced to the GC, using relative response factors of individual C_2–C_5 gases to methane predetermined from a standard mixture of C_1–C_5 gases.

The stable carbon isotope ratios of hydrocarbon gases were measured using a Mat 253 mass spectrometer interfaced to Trace GC Ultra. The GC was fitted with a HP-PLOT/Q capillary column (30 m × 0.32 mm × 20 μm) and helium was used as carrier gas. The temperature was kept constant at 50 °C (3 min hold), then increased to 190 °C (20 min hold) at 15 °C/min. At least two measurements were performed for each gas sample to confirm that errors were less than ±0.5‰. The isotope values were calibrated against the reference gas and are reported in the usual delta notation relative to VPDB.

3. Results

3.1. Gas yields

The gas yields from the pyrolysis experiments are presented in Table 1 and Figure 3. At each pressure, as expected, the total hydrocarbon gas (C_1–C_5), methane, and wet gas yields (C_2–C_5) show a continuous increase with increasing temperature.

However, the gas yields increased much more with increasing temperatures at 200 bar compared to higher liquid-water pressures (470, 750 and 900 bar). For example, as the temperature increased from 350 to 425 °C, the total hydrocarbon gas yield increased from 4.0 to 180 mg/g.oil at 200 bar, compared to 0.6 to 88 mg/g.oil at 470 bar.

As shown in Figure 3, at the same temperature, the C_1–C_5 total gas yields are higher at low pressure (200 bar) than at the higher pressures (470–900 bar), although different trends are evident at the different temperatures. At 350 and 373 °C, C_1–C_5 yields are 4.0 and 15.5 mg/g.oil at 200 bar, respectively. The yields are reduced by 91% to 0.35 mg/g.oil and 82% to 2.7 mg/g.oil at 900 bar when compared to the amount generated at 200 bar. At 390 °C, the C_1–C_5 yield is reduced by 74% as the pressure increased from 200 (35.0 mg/g.oil) to 750 bar (9.1 mg/g.oil). However, the C_1–C_5 yield is slightly higher at 900 bar (15.0 mg/g.oil) compared to that at 750 bar. At the higher temperatures of 405 and 425 °C, as the pressure increases from 200 to 470 bar, C_1–C_5 yields are reduced by 61% from 77.9 to 30.7 mg/g.oil and by 51% from 180.4 to 88.4 mg/g.oil, respectively. Then the gas yields rise by 29% at 405 °C and 49% at 425 °C with the increase in pressure to 750 bar compared to 470 bar. But at 900 bar, the C_1–C_5 yields are consistent with or slightly reduced compared to 750 bar. The unsaturated alkenes yields are highest at 200 bar, but decrease significantly with the higher water pressures (Table 1, Figure 4a) as found in all previous studies with high pressure.[16, 31, 32] Overall, there are no obvious yield trends associated with the phase change of water going from 350 to 405 °C through the supercritical temperature of 373 °C.

The yields of non-hydrocarbon gas (CO_2 and H_2) are usually low in oil cracking experiments (Table 1, Figure 4a, b). The highest yield is 0.07 mg/g.oil at 200 bar and

405 °C for H_2 and 9.2 mg/g.oil at 750 bar and 425 °C for CO_2. As shown in Figure 4b, at 350 to 405 °C, the CO_2 yields decrease as pressure increases from 200 to 900 bar. However, at 425 °C, the CO_2 yields remain nearly constant with increasing pressure in the range of 7.5 to 9.2 mg/g.oil. A significant fraction of the CO_2 dissolves in the water, which might account for some of these variations. The H_2 yields decrease with increasing pressure from 200 to 900 bar at 350 to 390 °C, except for the abnormal low yield at 200 bar and 373 °C (Figure 4a). At the higher temperatures of 405 and 425 °C, the H_2 yields are scattered with the yields at 750 bar being higher than at 470 bar.

3.2. Stable carbon isotopic compositions of individual gas component

Measured carbon isotope ratios for individual gas components from the oil cracking experiments are presented in Table 2 and Figure 5. The $\delta^{13}C$ values of methane, ethane, propane and butane show a "normal" isotope distribution with $\delta^{13}C_1 < \delta^{13}C_2 < \delta^{13}C_3 < \delta^{13}C_4$ at the same level of thermal maturity. For example, the carbon isotope ratio of methane is about -47.1 to-45.0‰ at 373 °C in the pressure range of 200 to 900 bar, while the carbon isotope ratio of -37.1 to -36.4‰ for ethane and -34.1 to 33.8‰ for propane show an enrichment of ^{13}C in comparison with methane. This "normal" distribution is in agreement with conventional thermogenic natural gas[36, 37] and pyrolysis results of kerogen, coal and oil.[38, 39]

Stable carbon isotopic curves of the different gas components change to differing extents with increasing pressure. For methane, the isotope ratio at 350 °C shows little variation (-46.3 to -45.4‰) over the pressure range of 200 to 900 bar. At the higher temperatures of 373 to 425 °C, the isotope ratios show a continuous increase in ^{13}C as pressure increases, with the maximum carbon isotope fractionation being about 2‰ at

373 °C and 3‰ at 390 to 425 °C. For ethane and propane, the isotopic compositions are more enriched in ^{13}C with increasing pressure at 350–405 °C, but the isotopic fractionations are less than ~1‰ (within the analytical precision of ±0.5‰). At 425 °C, ethane and propane are depleted in ^{13}C as pressure increases. For butane, the isotope ratio at 350 °C shows abnormal enrichment in ^{13}C with an isotopic fractionation of 3.3‰ from 200 to 900 bar. At temperatures of 373–405 °C, the carbon isotopic fractionation is less than 1‰ with increasing pressure. At 425 °C, butane is depleted in ^{13}C as pressure increases, which is similar to that of ethane and propane. For pentane, the isotopic fractionations with increasing pressure are in the range of 1.3 to 2.7‰ at different temperatures, which are greater than the other wet gas components.

The carbon isotope ratios for iC$_4$ and iC$_5$ tend to be less negative with increasing pressure at a given temperature, and the corresponding isotopic fractionations are higher than that of the *n*-alkane gas component with same carbon number. Carbon isotope ratios for CO_2 at 200 bar at various temperatures are more enriched in ^{13}C compared to the high water-pressure experiments. However, the CO_2 isotopic composition for the 405 °C experiment shows abnormal enrichment in ^{12}C at 200 bar compared to that at high water pressure, which needs further validation.

4. Discussion

4.1 Pressure effects on gas yields

The extent of oil cracking can be directly measured by the yield of generated gas, and previous studies suggest that it can be most appropriately characterized by mass

yield of total gas.[12, 40] Therefore, the mass yield was employed here to investigate the effect of pressure on gas generation in the confined system used.

As showed in Figure 3, although the total hydrocarbon gas yields continuously increase with increasing temperature, the yields under low pressure (200 bar) are notably higher than those under high liquid pressure (470, 750, 900 bar), indicating that pressure suppresses oil cracking. However, the extent and mechanism of pressure retardation on oil cracking stage strongly depend on the thermal stage of evolution (Figure 3). At the peak oil to early wet gas stage (350 and 373 °C, equivalent vitrinite reflectance of 0.92 and 1.15 %, respectively), there is insufficient molecules/radicals to reach the high activation energy barriers for complete decomposition of free radicals,[31, 41] leading to the radicals tending to recombine in chain termination reactions. Increased pressure allows the free radicals to become longer or polymerize due to increased collision rates among reactants, resulting in decreased reaction rates, and thereafter suppression of gas generation (Figure 3). However, at the elevated stage in the wet gas window (390, 405 and 425 °C, 1.35–1.85% R_o), the kinetic energy of molecule/species is enough to overcome the reaction barrier.

At 390 °C, the pressure at first suppresses oil cracking to gas from 200 to 470 bar, followed by increasing in yield from 470 to 900 bar. At 405 °C and 425 °C, the pressure at first suppresses oil cracking to gas, but then demonstrates a significant increase in yield from 470 to 750 bar, followed by a steady state at 900 bar. Activation volume effects could account for the changes in oil cracking rates in high water-pressure range at the elevated stage in the wet gas window. Theoretically, the collision rates among reactants at the elevated stage in the wet gas window become more intense than that at the peak oil generation stage. When pressure increases, the

reaction rates will decrease due to changes in the thermodynamic stability of activated complex intermediates as well as cage and diffusional effects.[41] The model of activation volume is included to account for such effects, which has been elaborated in the previous works.[31, 42] Thus, the gas yields at 470-900 bars are lower than at 200 bar. On the other hand, concentrations and collision rates of reactants would be enhanced with increasing pressure, resulting in increased overall reaction rates.[31] Although cage/diffusional effects generally retard reaction rates with increasing pressure, collision rates among reactants will increase with pressure and reach a maximum at a given pressure threshold, resulting in increased reaction rates and gas yields.[31] This could be the case in this study, which shows higher yields at 750 bar than at 470 bar when oil cracks at the elevated stage in the wet gas window. We speculate that overall reaction rates at the elevated stage in the wet gas window mainly depend on competition between collision rates and cage/diffusional effects, but clearly further work is required.

The main source of CO_2 in pyrolysis experiments is from the decomposition of macromolecular organic matter (e.g., resins and asphaltenes), which contains oxygen functional groups. As shown in Figure 4b, similar to the pattern observed for hydrocarbon gas yields, pressure appears to retard cracking to CO_2. A significant decrease of CO_2 production occurs from 200 to 900 bar when the temperature is less than 425 °C. Due to low bond energies within macromolecules,[43, 44] 425 °C provides the thermal energy to enable the system to have sufficient energy for decomposition of macromolecules, accompanied by breakage and condensation of alkanes and aromatics. In this situation, the pressure effect is insignificant and subordinate to the temperature, and it is in agreement with the experimental results showing almost no change of CO_2 yield with increasing pressure at 425 °C. However, to further

substantiate these findings, the dissolved CO_2 in the aqueous phase after reaction needs to be measured. On the other hand, the phenomenon and mechanism of water acting as an external hydrogen source have been widely investigated and confirmed by the higher hydrocarbon gas yields and isotopic evidence.[45, 46] In addition, other studies suggested that oxygen also transfers from the water into the organic matter, as the amounts of CO_2 produced from hydrous pyrolysis experiments are higher than that under anhydrous conditions.[47, 48] However, the amount of CO_2 were not recorded in many experiments and few isotopic evidence had been published. Therefore, water-derived oxygen may transfer to the CO_2, but the evidence remains inconclusive and it needs more in-depth work to verify the possibility of external oxygen source for CO_2 during pyrolysis.

4.2 Pressure effects on gas molecular parameters

The gas dryness coefficients ($C_1/\Sigma C_{1-5}$ volume %) presented in Table 3 and Figure 6a decrease with increasing thermal stress at any given pressure. This is in agreement with previous studies by Tian et al.[49] and Hill et al.[24] who found that the maximum C_2–C_5 gas yield occurs at an equivalent %R_o value of 1.9–2.0% in sealed gold-tube experiments with constant pressure, suggesting that heavy gas component (C_2–C_5) cracking starts at an equivalent %R_o value of ~2.0%. EasyR_o calculations for the temperature setup here show that the maximum thermal stress reached during experiments is at equivalent %R_o value of ~1.85%, which is on the threshold of C_2–C_5 cracking. Therefore, secondary cracking of heavy gas components has less influence on the dryness coefficient trends in the experimental temperature range investigated here, and the heavy components in crude oil are the main contributors to the hydrocarbon gases.

However, the dryness coefficient continuously increases with pressure from 200 to 470 bar at any temperature, and almost stays constant as pressure increases from 470 to 900 bar, suggesting pressure effects on the generation of the different gas components. This is clearly indicated by the difference in the generation rates of methane and C_2–C_5 wet gas components. At 405 and 425 °C, almost no change in $Ln(C_1/C_2)$ is observed over the pressure range investigated, indicating that generation rates of methane and the C_2–C_5 wet gas components are comparable with temperature playing the dominant role in oil cracking. Conversely, at lower temperatures (350, 373 and 390 °C), pressure has a major influence on the generation rates of individual gas components. Compared to the C_2–C_5 wet gas components, methane has a faster generation rate as revealed by the increasing $Ln(C_1/C_2)$ value with increasing pressure (Figure 6b). We speculate that more intense radical collisions at high water pressure result in enhanced generation of methane to account for the increasing dryness coefficient. Furthermore, the higher slope of the $Ln(C_1/C_2)$ values under high water pressure (470, 750 and 900 bar) with temperature reveals a much greater difference in the generation rate between methane and the C_2–C_5 wet gas components compared to low pressure conditions (Figure 6b). Thus, increasing gas dryness coefficients have been obtained with increasing pressure upon thermal evolution (Figure 6a). For example, at a pressure of 200 bar, no more than 10% difference in dryness is observed across the temperature range, compared to ~25% at 750 bar. The results suggest that both thermal maturation and pressure control gas dryness coefficients, but clearly the values are strongly dependent on the thermal stage of evolution.

The ratios of iC$_4$/nC$_4$ and iC$_5$/nC$_5$ increase consistently with pressure, except for decreases at 900 bar for some temperatures (Figure 6c). Previous studies showed that normal alkanes are formed by free radical reactions during petroleum formation, but

branched isomeric alkanes, in addition to free radical cracking, are formed by carbonium ion reactions of α-olefins with protons, which are promoted under acidic conditions.[50-52] Although the yields of molecular hydrogen and alkene gases are usually low in closed pyrolysis experiments,[24, 53, 54] the H_2 yields at low pressures here are generally higher than at high pressures. Similarly, the butene yields are highest at 200 bar and then decrease as pressure increases to 900 bar, as shown in Figure 4a. Interestingly, the ratios of butene/butane show a steady decrease as pressure increases from 200 to 900 bar (Figure 6d). This suggests that reactions occur between hydrogen and unsaturated alkene gases, or in other words, increased pressure promotes hydrogenation of alkene gases to saturated alkane gases.[31] Therefore, it is possible that free radical cracking of branched components could account for branched isomeric alkane formation in our experiments. However, free radical cracking seems to be retarded with increasing pressure, as the alkane yields are lower at high pressure Recently, Xia et al.[55] suggested that *iso*-alkanes are not necessarily derived from *iso*-alkyl precursors, they may also be the product of normal alkyl radicals after rearrangement (e.g., by a methyl shift). Pressure may be beneficial for the rearrangement reaction, leading to increased isomeric/normal alkane ratios as revealed by iC_4/nC_4 and iC_5/nC_5 values in Figure 6c. As shown in Figure 4a, decreasing trend of alkenes yield as pressure increases might be related to the generation reactions. This is partly because increased pressure enhances completion of alkenes reactions, including the hydrogenation to saturated alkane gases. However, lack of alkenes in natural gases is probably not an indicator of high pressure conditions. The lack of alkenes might indicate that alkenes never form during petroleum generation and oil-cracking or that alkenes react very quickly if they are formed. Alkenes are known to be artifacts in pyrolysis experiment as revealed by many previous studies. The

presence of small amounts of alkenes may be due to the differences between short time laboratory experiments and the extremely long time-scales for many geological processes.[56]

4.3 Pressure effects on carbon isotopic composition of gas components

Stable carbon isotope geochemistry of hydrocarbon gases has proved to be a powerful tool to determine the gas genetic types, source and accumulation history. Although many studies show that pressure retards organic maturation and thermal cracking, few studies show pressure effects on stable carbon isotopic fractionation of individual gas components. Previously, Hill et al.[31] found ~2‰ fractionation of methane carbon isotopes with pressure ranging from 90 to 2000 bar at 380 °C in sealed gold-tube oil cracking experiments, suggesting that pressure may have important influence on isotope fractionation. However, the methane carbon isotope value in their study showed fractionation within ~1‰ with increasing pressure, except one measured data point at 1380 bar which became enriched in ^{13}C. In Figure 7a, b and c, the $\delta^{13}C$ values of C_1–C_5 gases at the four different pressures in our experiment are plotted on "natural gas plots" (after Chung et al.[37]) who proposed that $\delta^{13}C$ values of different gas compounds are linearly related to the inverse of their respective carbon numbers ($1/C_n$). The carbon isotope values of ethane, propane and butane show a maximum variation of ~1‰ as pressure increases, indicating that pressure has little effect on carbon isotope ratios of the normal C_2–C_4 alkane gas components. However, a maximum isotopic fractionation of ~3.5‰ for methane is observed over the pressure range (200 to 900 bar) investigated in our experiments. The difference in methane carbon isotopic fractionation for the two oils used in our study and Hill et al.[31] is more likely due to potential differences in oil composition. The oil used by Hill

et al. was saturate rich (63.8% saturates, 22.9% aromatics, 6.6% resins, 6.7% asphaltenes)[31] and was not biodegraded while the oil used here is slightly biodegraded being more enriched in resins and asphaltenes. If we consider the number of different sources for methane from oil, differences in methane carbon isotopes should be possible.

It is well known that the isotope ratios of gas components are controlled not only by the isotopic compositions of precursors, but also the temperature and mechanism of gas generation, and the conversion is the key factor to determine the evolution of methane isotopic composition.[28, 57] Surprisingly, the heaviest methane carbon isotope ratio does not coincide with the maximum gas yield due to pressure retardation on oil cracking (Figure 3). One possibility is that pressure affects methane carbon isotope fractionation by influencing the rates of various methane generation reactions differently. Based on kinetic modelling of $\delta^{13}C_1$ and activation energy, Shuai et al.[57] also suggest that the pressure affects isotope ratios of methane mainly through methane generation. Both iC$_4$ and iC$_5$ generally show enrichment in ^{13}C with increasing pressure (Table 2). As shown in Figure 6c, increased pressure seems to favor the generation of *iso*-alkanes due to enhanced rearrangement of normal alkyl radicals. It is possible that *iso*-alkanes start to crack at higher temperature of 425°C, which may affect the isotopic fractionation. However, the carbon isotopes of *iso*-alkanes show good correlations with *iso*-alkane/normal alkane ratios, suggesting that isomerization may be the principal factor controlling the isotopic fractionation of *iso*-alkanes, and cracking is comparatively less important. The pressure effect on the carbon isotope ratios for iC$_5$ is less distinct when temperature increases (Table 2), suggesting that temperature plays a major role in oil cracking at the later stages in the wet gas window.

Overpressure is evident in many petroliferous basins. In these basins, retardation of vitrinite reflectance values might be recognized in source rocks, thus influencing the estimated depth of the oil window. The suppression effect of pressure on oil cracking from this study implies that pressure could be a significant control on thermal stability of crude oil in deep strata. Our experiments clearly show that pressure has a major influence on gas yield, the rate of formation of individual gases, and carbon isotope compositions of methane. It should be with caution when the methane isotope data from deep-buried strata are interpreted. Due to the significant differences in methane carbon isotopes between pressurized and normal oil cracking, the carbon isotope curve based on C_1–C_5 isotope ratios could provide a potential guide to identify pressure effects on *in-situ* oil cracking in deep strata. We have constructed a conceptual model using the "natural gas plot" for this application (Figure 7d). Of course, the kinetics of isotope fractionation must be defined when extrapolating this conceptual model to geological basins.

4.4 Water phase effect on pressurized oil-cracking

Because most of the simulation experiments in previous work were conducted in the presence of liquid water or two-phases of liquid and vapor, the role of supercritical fluid water phase during high temperature experiments remains inconclusive, leading to the uncertainty of the conclusion in this study. It is well known that supercritical water has the characteristics of favorable transport properties and high diffusivities, which are different from the liquid water phase.[58, 59] To investigate the effect of water with different phases on gas generation in pressurized oil cracking, a series of pyrolysis experiments were conducted in a confined system (gold tubes) using the same crude oil under anhydrous and hydrous conditions, at a

fixed pressure of 450 bar and for 24 hours. Temperatures points were set at 370, 390 and 405 °C (accuracy ±1 °C). The oil/water is 1:5 (w/w) in pyrolysis experiments. The water occurs in normal phase at 370 °C and in supercritical fluid phase at 390 and 405 °C. Yields and measured carbon isotope values of gas components in three comparative experiments are presented in Table 4, Figure 8 and 9. The methane yields are almost same between the anhydrous and hydrous pyrolysis at all three temperature-settings. However, the yields of C_2^+ components are significantly higher in hydrous pyrolysis compared to under anhydrous conditions, further indicated by the higher wetness of ($\Sigma C_{2-5}/\Sigma C_{1-5}$). The results demonstrate that the water promotes wet gas generation with no significant change on methane generation. Interestingly, the CO_2 yields show a similar trend to that of the wet gases, probably an indicative of the same promotion effect of CO_2 generation as for the C_2^+ components. No significant change in the $\delta^{13}C$ values of each gas components and CO_2 between anhydrous and hydrous pyrolysis is observed at all three temperatures, except for the carbon isotopes of *i*-C_5 and C_5 at 425 °C, suggesting that supercritical water above 374 °C does not have a significant effect on the hydrocarbon-cracking reaction pathway. This is in agreement with a previous study by Liu et al.[60] who concluded that upgrading of residual oil in sub- and supercritical water is still dominated by free radical reaction mechanisms. Although supercritical conditions are clearly not encountered in natural oil reservoirs, the oil-cracking experiments under high water pressures and high temperatures here still can be used to evaluate the pressure effect on gas generation during oil cracking processes.

5. Conclusions

Oil-to-gas cracking was observed to be generally retarded by pressure, and the extent of retardation strongly depends on the stage of thermal evolution. In the early

stage of maturation using temperatures of 350 and 373 °C (EasyR_o = 0.92–1.15%), increasing pressure retards the gas yields. At 390 °C (EasyR_o = 1.35%), gas yields were retarded by pressure from 200 to 470 bar, followed by a slight increase going from 470 to 900 bar. For the highest maturity stage at 405 and 425 °C (EasyR_o = 1.56–1.85%), gas yields were retarded at pressures from 200 to 470 bar, weakly promoted from 470 to 750 bar, and stabilized from 750 to 900 bar. The competition between cage/diffusional effects with the collision rates of reactants could account for the relatively reaction rates leading to gas formation changing with pressure.

The gas dryness coefficient continuously increased with pressure from 200 to 470 bar at all temperatures investigated and then stayed nearly constant as pressure was further increased to 900 bar. Thus, the generation rates of methane and the C_2–C_5 wet gas components differ at lower thermal stress before becoming comparable at higher levels.

As for the gases generated, methane was enriched in ^{13}C by up to 3‰ from 200 to 900 bar. However, the carbon isotope ratios for ethane, propane and butane showed little variation (less than 1‰) with increasing pressure. A conceptual model using "natural gas plot" was constructed to identify pressure effect on *in-situ* oil cracking. Supercritical water above 374 °C did not make significant effect on the hydrocarbon-cracking reaction pathways of oil-to-gas in closed systems, as revealed by yields and isotopes under hydrous and anhydrous pyrolysis being similar for the gold bag experiments.

Acknowledgements

This work was supported by the National Natural Science Foundation of China (41572101, 41330313), the Qingdao Doctoral Foundation (2015000114) and the

cooperative research grant from The University of Nottingham and Zhejiang University. We also thank Dr. Ken Peters and three anonymous reviewers for their constructive comments and suggestions, which significantly improved the quality of this manuscript.

References

(1) Hunt, M. *Petroleum Geochemistry and Geology*; WH Freeman and Company: San Francisco, 1979; pp 466.

(2) Tissot, B. P.; Welte, D. H. *Petroleum Formation and Occurrence. (2nd ed)*; Berlin-Heidelberg-New York: Springer-Verlag, 1984; pp 1–699.

(3) Price, L. C. *Geochim. Cosmochim. Acta* **1993**, *57*, 3261–3280.

(4) McNeil, R. I.; Bement, W. O. *Energy Fuels* **1996**, *10*, 60–67.

(5) McTavish, R. *J. Petrol. Geol.* **1998**, *21*, 153–186.

(6) Huijun, L.; Tairan, W.; Zongjin, M.; Wencai, Z. *Mar. Petrol. Geol.* **2004**, *21*, 1083–1093.

(7) Hao, F.; Zou, H.; Gong, Z.; Yang, S.; Zeng, Z. *AAPG Bull* **2007**, *91*, 1467–1498.

(8) Carr, A. *Mar. Petrol. Geol.* **1999**, *16*, 355–377.

(9) Mi, J.; Zhang, S.; He, K. *Org. Geochem.* **2014**, *74*, 116–122.

(10) Monthioux, M.; Landais, P.; Durand, B. *Org. Geochem.* **1986**, *10*, 299–311.

(11) Huang, W.-L. *Org. Geochem.* **1996**, *24*, 233–241.

(12) Schenk, H.; Di Primio, R.; Horsfield, B. *Org. Geochem.* **1997**, *26*, 467–481.

(13) Price, L. C.; Wenger, L. M. *Org. Geochem.* **1992**, *19*, 141–159.

(14) Zou, Y.; Peng, P. *Mar. Petrol. Geol.* **2001**, *18*, 707–713.

(15) Uguna, C. N.; Snape, C. E.; Meredith, W.; Carr, A. D.; Scotchman, I. C.; Davis, R. C. *AAPG Hedberg Series* **2012**, 19–37.

(16) Uguna, C. N.; Carr, A. D.; Snape, C. E.; Meredith, W. *Org. Geochem.* **2015**, *78*, 44–51.

(17) Hryckowian, E.; Dutcher, R. R.; Dachille, F. *Econ. Geol.* **1967**, *62*, 517–539.

(18) Braun, R. L.; Burnham, A. K. *Energy Fuels* **1990**, *4*, 132–146.

(19) Tao, W.; Zou, Y.; Carr, A.; Liu, J.; Peng, P. *Fuel* **2010**, *89*, 3590–3597.

(20) Goodarzi, F. *Fuel* **1985**, *64*, 156–162.

(21) Behar, F.; Vandenbroucke, M. *Energy Fuels* **1996**, *10*, 932–940.

(22) Carr, A.; Snape, C.; Meredith, W.; Uguna, C.; Scotchman, I.; Davis, R. *Petrol. Geosci.* **2009**, *15*, 17–26.

(23) Ungerer, P.; Behar, F.; Villalba, M.; Heum, O. R.; Audibert, A. *Org. Geochem.* **1988**, *13*, 857–868.

(24) Hill, R. J.; Tang, Y. C.; Kaplan, I. R. *Org. Geochem.* **2003**, *34*, 1651–1672.

(25) Tang, Y.; Huang, Y.; Ellis, G. S.; Wang, Y.; Kralert, P. G.; Gillaizeau, B.; Ma, Q.; Hwang, R. *Geochim. Cosmochim. Acta* **2005**, *69*, 4505–4520.

(26) Dominé, F. *Energy Fuels* **1989**, *3*, 89–96.

(27) Dominé, F. *Org. Geochem.* **1991**, *17*, 619–634.

(28) Lorant, F.; Behar, F.; Vandenbroucke, M.; McKinney, D. E.; Tang, Y. *Energy Fuels* **2000**, *14*, 1143–1155.

(29) Jackson, K. J.; Burnham, A. K.; Braun, R. L.; Knauss, K. G. *Org. Geochem.* **1995**, *23*, 941–953.

(30) Fabuss, B.; Smith, J.; Satterfield, C. *Adv. Pet. Chem. Refin.* **1964**, *9*, 157–201.

(31) Hill, R. J.; Tang, Y.; Kaplan, I. R.; Jenden, P. D. *Energy Fuels* **1996**, *10*, 873–882.

(32) Uguna, C. N.; Carr, A. D.; Snape, C. E.; Meredith, W.; Castro-Díaz, M. *Org. Geochem.* **2012**, *52*, 103–113.

(33) Michels, R.; Landais, P.; Torkelson, B.; Philp, R. *Geochim. Cosmochim. Acta* **1995**, *59*, 1589–1604.

(34) Lewan, M. D. In *Organic geochemistry, principles and applications*; Engel, M. H., Macko, S. A., Eds.; Plenum: New York, 1993; pp 419–442.

(35) Sweeney, J. J.; Burnham, A. K. *AAPG Bull.* **1990**, *74*, 1559–1570.

(36) Schoell, M. *AAPG Bull.* **1983**, *67*, 2225–2238.

(37) Chung, H. M.; Gormly, J. R.; Squires, R. M. *Chem. Geol.* **1988**, *71*, 97–104.

(38) Andresen, B.; Throndsen, T.; Råheim, A.; Bolstad, J. *Chem. Geol* .**1995**, *126*, 261–280.

(39) Berner, U.; Faber, E.; Scheeder, G.; Panten, D. *Chem. Geol.* **1995**, *126*, 233–245.

(40) Tian, H.; Xiao, X.; Wilkins, R. W.; Tang, Y. *Org. Geochem.* **2012**, *46*, 96–112.

(41) Mallinson, R. G.; Braun, R. L.; Westbrook, C. K.; Burnham, A. K. *Ind. Eng. Chem. Res.* **1992**, *31*, 37–45.

(42) Al Darouich, T.; Behar, F.; Largeau, C. *Org. Geochem*. **2006**, *37*, 1155–1169.

(43) Ranjbar, M.; Pusch, G. *J. Anal. Appl. Pyrol.* **1991**, *20*, 185–196.

(44) Karacan, O.; Kok, M. V. *Energy Fuels* **1997**, *11*, 385–391.

(45) Hoering, T. C. *Org. Geochem*. **1984**, *5*, 267–278.

(46) Schimmelmann, A.; Boudou, J.-P.; Lewan, M. D.; Wintsch, R. P. *Org. Geochem*. **2001**, *32*, 1009–1018.

(47) Helgeson, H. C.; Knox, A. M.; Owens, C. E.; Shock, E. L. *Geochim. Cosmochim. Ac*. **1993**, *57*, 3295–3339.

(48) Lewan, M. D. *Geochim. Cosmochim. Ac*. **1997**, *61*, 3691–3723.

(49) Tian, H.; Wang, Z.; Xiao, Z.; Li, X.; Xiao, X. *Chinese Sci. Bull* **2006**, *51*, 2763–2770.

(50) Alomon, W.; Johns, W. *Advance of Organic Geochemistry*; Enadimsa: Madrid, 1975; pp *157*–172.

(51) Kissin, Y. V. *Geochim. Cosmochim. Acta* **1987**, *51*, 2445–2457.

(52) Pan, C.; Geng, A.; Zhong, N.; Liu, J.; Yu, L. *Energy Fuels* **2008**, *22*, 416–427.

(53) Behar, F.; Vandenbroucke, M.; Teermann, S.; Hatcher, P.; Leblond, C.; Lerat, O. *Chem. Geol.* **1995**, *126*, 247–260.

(54) Pan, C.; Jiang, L.; Liu, J.; Zhang, S.; Zhu, G. *Org. Geochem.* **2010**, *41*, 611–626.

(55) Xia, X. *Org*. *Geochem*. **2014**, *74*, 143–149.

(56) Saxby, J. D.; Bennett, A. J. R.; Corcoran, J. F.; Lambert, D. E.; Riley, K. W. *Org*. *Geochem*. **1986**, *9*, 69–81.

(57) Shuai, Y.; Peng, P.; Zou, Y. *Fuel* **2006**, *85*, 860–866.

(58) Siskin, M.; Katritzky, A. R. *Chem*. *Rev*. **2001**, *101*, 825–836.

(59) Tsuzuki, N.; Takeda, N.; Suzuki, M.; Yokoi, K. *Int*. *J. Coal Geol*. **1999**, *39*, 227–250.

(60) Liu, Y.; Bai, F.; Zhu, C.-C.; Yuan, P.-Q.; Cheng, Z.-M.; Yuan, W.-K. *Fuel Process*. *Technol*. **2013**, *106*, 281–288.

Table captions

Table 1. Gas yields from the oil cracking experiments at different temperatures and pressures.

Table 2. Stable carbon isotopic compositions of individual gas components from the oil cracking experiments.

Table 3. Molecular parameters for hydrocarbon gases obtained from oil cracking at different temperatures and pressures.

Table 4. Gas yields (mg/g) and stable carbon isotopic compositions of individual gas components from the oil cracking experiments in gold capsules.

Figure captions

Figure 1. Whole oil gas chromatogram of crude oil from the Pearl River Mouth Basin, South China Sea, and its composition by compound class. Pr: pristane; Ph: phytane.

Figure 2. Schematic diagram of the pyrolysis apparatus (after Uguna *et al.*[16]).

Figure 3. Yields of total hydrocarbon gases (C_1–C_5) produced by oil cracking at different temperatures and pressures.

Figure 4. Yields of (a) hydrogen and propene and (b) CO_2 obtained from oil cracking at different temperatures and pressures.

Figure 5. Carbon isotope ratios of individual hydrocarbon gas components with increasing pressure at different temperatures.

Figure 6. Changes in molecular parameters for hydrocarbon gases with increasing temperature and pressure. (a) dryness ($C_1/\Sigma C_{1-5}$ volume); (b) Ln(C_1/C_2 volume); (c) *iso*-/normal alkane; (d) butene/butane.

Figure 7. "Natural gas plot" of $\delta^{13}C(C_n)$ versus $1/C_n$ (after Chung *et al.*[37]). (a) 373 °C; (b) 390 °C; (c) 425 °C; (d) the overall conceptual model showing the effect of pressure.

Figure 8. Gas yields (mg/g) of individual gas components from the oil cracking experiments in gold capsules, in the presence and absence of water. (a) 370 °C; (b) 390 °C; (c) 425 °C.

Figure 9. **S**table carbon isotopic compositions of individual gas components from the oil cracking experiments in gold capsules, in the presence and absence of water. (a) 370 °C; (b) 390 °C; (c) 425 °C.

Table 1. Gas yields from the oil cracking experiments at different temperatures and pressures.

Temperature	Pressure [a] (bar)	Yields of gas produced from oil cracking (mg/g. oil)												
		CH_4	C_2H_4	C_2H_6	C_3H_6	C_3H_8	C_4 alkenes	C_4 alkanes	C_5 alkenes	C_5 alkanes	H_2	CO_2	ΣC_{1-5}	ΣC_{2-5}
350 °C 0.92%R_o	200/175	1.2	0.07	0.67	0.22	0.78	0.18	0.43	0.09	0.29	0.032	2.09	4.0	2.73
	470/431	0.25	<0.01	0.10	0.01	0.08	<0.01	0.06	<0.01	0.08	0.011	0.51	0.58	0.33
	750/745	0.25	<0.01	0.09	0.01	0.06	<0.01	0.05	<0.01	0.06	0.012	0.48	0.51	0.26
	900/879	0.15	<0.01	0.05	0.02	0.04	<0.01	0.03	<0.01	0.07	0.012	0.30	0.35	0.21
373 °C 1.15%R_o	200/190	4.5	0.18	2.9	0.73	3.31	0.58	1.9	0.37	1.00	0.001	2.91	15.5	11.0
	470/485	1.3	0.02	0.73	0.06	0.58	0.04	0.32	0.01	0.14	0.011	0.79	3.2	1.9
	750/759	1.3	0.02	0.62	0.04	0.47	0.03	0.31	0.01	0.15	0.014	0.58	2.9	1.6
	900/821	1.2	0.01	0.58	0.03	0.44	0.02	0.24	<0.01	0.12	0.013	0.65	2.7	1.4
390 °C 1.35%R_o	200/223	9.6	0.29	7.6	1.5	8.1	1.18	4.28	0.72	1.86	0.043	3.74	35.0	25.4
	470/469	3.1	0.05	1.97	0.12	1.5	0.08	0.96	0.03	0.27	0.017	3.33	8.1	5.0
	750/738	3.6	0.04	2.24	0.10	1.7	0.07	1.04	0.02	0.29	0.018	1.13	9.1	5.5
	900/890	5.4	0.04	3.16	0.10	2.85	0.08	2.59	0.03	0.69	0.017	1.40	15.0	9.6
405 °C 1.56%R_o	200/215	19.7	0.31	18.7	2.2	19.6	2.0	10.2	1.14	4.10	0.065	5.82	77.9	58.2
	470/462	9.0	0.09	8.1	0.39	7.29	0.30	4.46	0.09	0.98	0.026	2.77	30.7	21.7
	750/769	11.8	0.06	9.8	0.25	9.14	0.21	6.67	0.07	1.70	0.052	3.27	39.7	27.9
	900/890	10.6	0.06	9.3	0.32	9.07	0.31	6.37	0.13	1.74	0.027	2.73	37.9	27.3
425 °C 1.85%R_o	200/210	45.5	0.33	47.2	2.7	48.5	2.7	24.8	1.3	7.55	0.057	8.3	180.4	134.9
	470/510	25.9	0.14	23.1	0.55	22.1	0.47	12.8	0.16	3.12	0.038	7.5	88.4	62.5
	750/745	34.7	0.09	29.7	0.38	33.6	0.44	26.1	0.25	6.84	0.054	9.2	132.0	97.3
	900/897	33.0	0.10	30.0	0.47	33.4	0.53	22.7	0.29	5.62	0.051	8.4	126.1	93.1

[a] The pressure is listed as the set pressure / measured pressure.

Table 2. Stable carbon isotopic compositions of individual gas components from the oil cracking experiments.

Temperature	Pressure[a] (bar)	$\delta^{13}C$ (‰)							
		C_1	C_2	C_3	iC_4	C_4	iC_5	C_5	CO_2
350 °C 0.92%R_o	200/175	-45.6	-36.5	-34.1	-33.5	-31.7	-29.6	-29.7	-29.2
	470/431	-45.4	-36.0	-33.7	-31.9	-29.2	-25.4	-27.0	-23.7
	750/745	-46.3	-35.6	-33.3	-31.7	-29.2	-24.4	-27.0	-24.6
	900/879	-45.6	-35.7	-33.8	-31.7	-28.4	-24.9	-27.6	-22.9
373 °C 1.15%R_o	200/190	-47.1	-36.6	-34.0	-34.0	-30.9	-30.4	-28.3	-29.0
	470/485	-45.6	-37.1	-34.1	-33.0	-30.9	-28.5	-27.8	-26.4
	750/759	-45.5	-36.5	-33.8	-32.1	-30.3	-26.7	-27.4	-25.9
	900/821	-45.0	-36.4	-33.9	-32.3	-30.6	-25.3	-27.0	-25.5
390 °C 1.35%R_o	200/223	-47.0	-36.7	-33.5	-34.0	-30.0	-29.6	-29.0	-28.6
	470/469	-44.8	-36.5	-33.0	-31.3	-29.6	-25.8	-27.0	-25.0
	750/738	-45.1	-36.5	-33.0	-31.2	-29.7	-26.6	-27.2	-25.1
	900/890	-44.2	-35.8	-32.7	-30.4	-29.9	-27.2	-27.5	-26.2
405 °C 1.56%R_o	200/215	-46.6	-35.6	-32.3	-33.0	-28.7	-28.3	-27.1	-24.9
	470/462	-46.7	-36.1	-31.8	-30.6	-27.9	-27.1	-25.7	-27.1
	750/769	-44.3	-35.0	-31.5	-29.4	-27.9	-26.4	-25.6	-27.1
	900/890	-44.4	-35.0	-31.5	-29.7	-28.0	-26.4	-26.0	-27.2
425 °C 1.85%R_o	200/210	-45.2	-33.2	-29.4	-31.0	-24.6	-24.1	-21.2	-28.8
	470/510	-42.8	-33.4	-29.5	-28.1	-24.9	-22.2	-20.9	-25.7
	750/745	-41.6	-33.6	-29.9	-27.8	-26.1	-22.9	-22.8	-26.6
	900/897	-42.5	-33.8	-29.9	-28.0	-25.9	-23.4	-23.3	-26.1

[a] The pressure is listed as the set pressure / measured pressure.

Table 3. Molecular parameters for hydrocarbon gases obtained from oil cracking at different temperatures and pressures.

Temperature	Pressure[a] (bar)	Molecular parameters				
		Ln(C_1/C_2 Volume)	$C_1/\Sigma C_{1-5}$ Volume%	butene/butane	iC_4/nC_4[b]	iC_5/nC_5[b]
350 °C 0.92%R_o	200/175	1.11	54.3	0.41	0.44	1.11
	470/431	1.50	67.1	0.07	0.88	1.65
	750/745	1.64	71.3	0.07	0.80	1.53
	900/879	1.65	68.0	0.00	1.07	3.40
373 °C 1.15%R_o	200/190	1.00	52.1	0.31	0.44	0.96
	470/485	1.16	62.3	0.12	1.26	1.86
	750/759	1.33	66.2	0.09	1.71	1.95
	900/821	1.35	67.5	0.08	1.40	1.83
390 °C 1.35%R_o	200/223	0.82	49.4	0.28	0.41	0.88
	470/469	1.05	60.3	0.08	1.75	2.59
	750/738	1.08	61.4	0.07	1.60	2.48
	900/890	1.15	59.5	0.03	2.78	3.62
405 °C 1.56%R_o	200/215	0.66	46.4	0.20	0.39	0.78
	470/462	0.72	50.7	0.07	1.42	2.48
	750/769	0.81	51.8	0.03	1.72	2.93
	900/890	0.76	50.0	0.05	1.45	2.49
425 °C 1.85%R_o	200/210	0.58	45.9	0.11	0.43	0.78
	470/510	0.74	50.8	0.04	1.02	2.04
	750/745	0.78	48.3	0.02	1.60	2.82
	900/897	0.72	47.7	0.02	1.30	2.41

[a] The pressure is listed as the set pressure / measured pressure.

[b] iC_4/nC_4 is the ratio of *iso*-butane to normal butane, and iC_5/nC_5 is the ratio of *iso*-pentane to normal pentane.

Table 4. Gas yields (mg/g. oil) and stable carbon isotopic compositions of individual gas components from the oil cracking experiments in gold capsules.

	Gas yields under different conditions (mg/g. oil)					
	370 °C		390 °C		405 °C	
	Oil + water	Oil	Oil + water	Oil	Oil + water	Oil
C_1	8.5	8.3	22.3	23.3	45.5	45.7
C_2	6.6	4.8	21.2	18.0	52.8	42.2
C_3	10.2	4.9	31.2	23.2	79.1	56.3
C_{4-5}	13.0	3.6	43.3	26.8	106.5	68.3
CO_2	5.8	3.7	8.3	5.1	14.3	5.9
ΣC_{2-5}	29.8	13.3	95.8	68.1	238.4	166.8
ΣC_{1-5}	38.3	21.6	118.1	91.3	283.9	212.5
wetness[a]	55.5	38.7	60.3	51.8	65.0	57.0
	$\delta^{13}C$ (‰)					
	373 °C		390 °C		405 °C	
	Oil + water	Oil	Oil + water	Oil	Oil + water	Oil
C_1	-46.5	-45.6	-45.5	-45.3	-45.0	-44.9
C_2	-36.2	-35.0	-35.1	-35.3	-34.1	-34.9
C_3	-33.1	-32.1	-31.4	-31.9	-29.9	-30.9
iC_4	-31.0	-30.2	-31.3	-31.0	-30.0	-29.8
C_4	-31.3	-30.4	-28.9	-29.9	-27.0	-28.2
iC_5	-28.5	-27.7	-26.5	-27.9	-23.9	-25.6
C_5	-28.8	-27.2	-26.8	-27.7	-23.4	-25.6
CO_2	-24.3	-24.7	-21.8	-22.2	-23.0	-21.8

[a] wetness= $\Sigma C_{2-5}/\Sigma C_{1-5}$ Volume%.

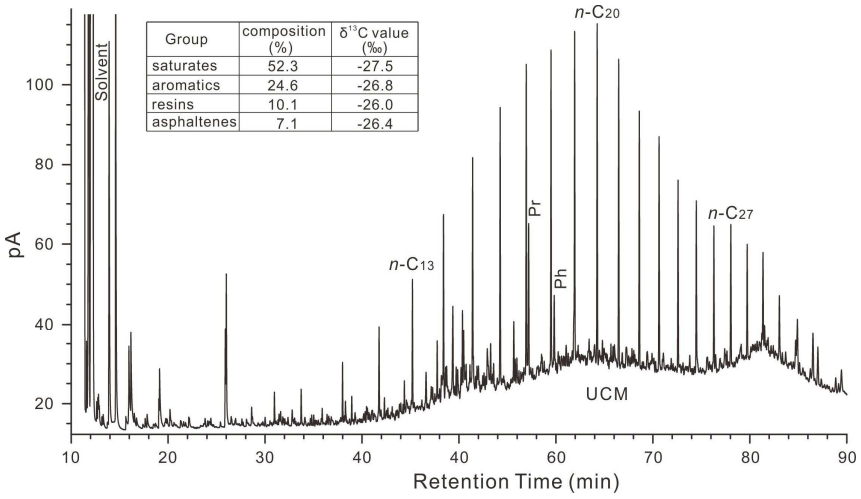

Figure 1. Whole oil gas chromatogram of crude oil from the Pearl River Mouth Basin, South China Sea, and its composition by compound class. Pr: pristane; Ph: phytane.

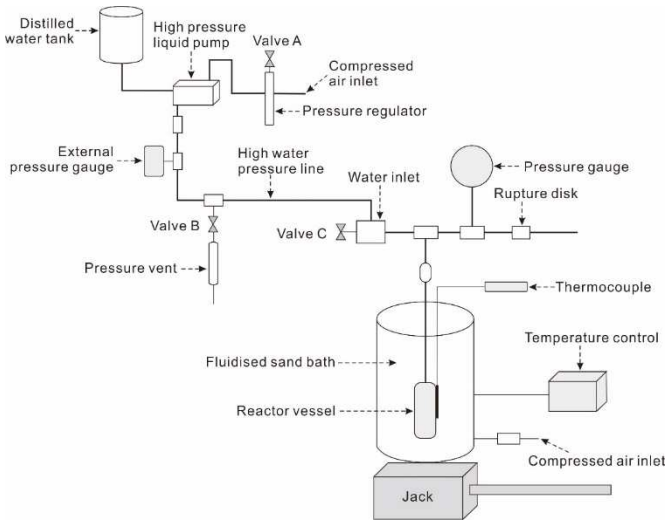

Figure 2. Schematic diagram of the pyrolysis apparatus (after Uguna *et al.*[16]).

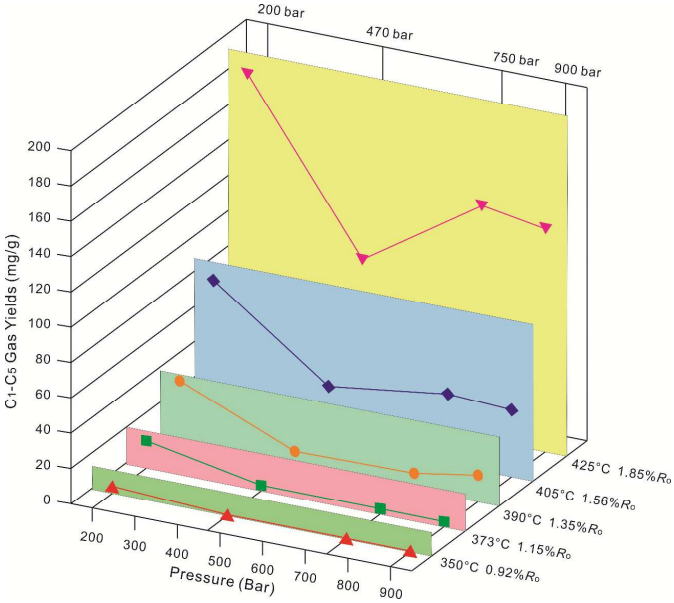

Figure 3. Yields of total hydrocarbon gases (C_1–C_5) produced by oil cracking at different temperatures and pressures.

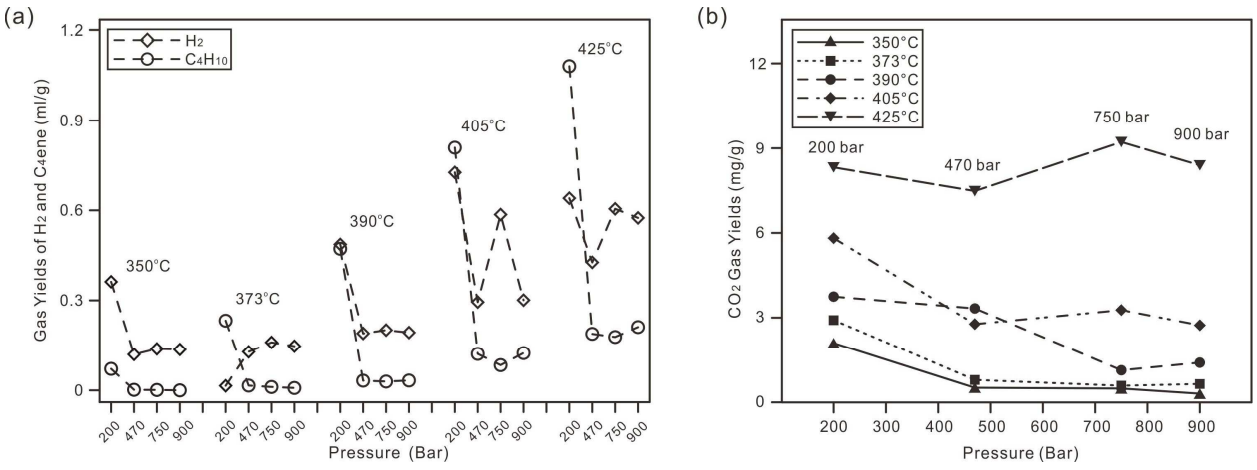

Figure 4. Yields of (a) hydrogen and propene and (b) CO_2 obtained from oil cracking at different temperatures and pressures.

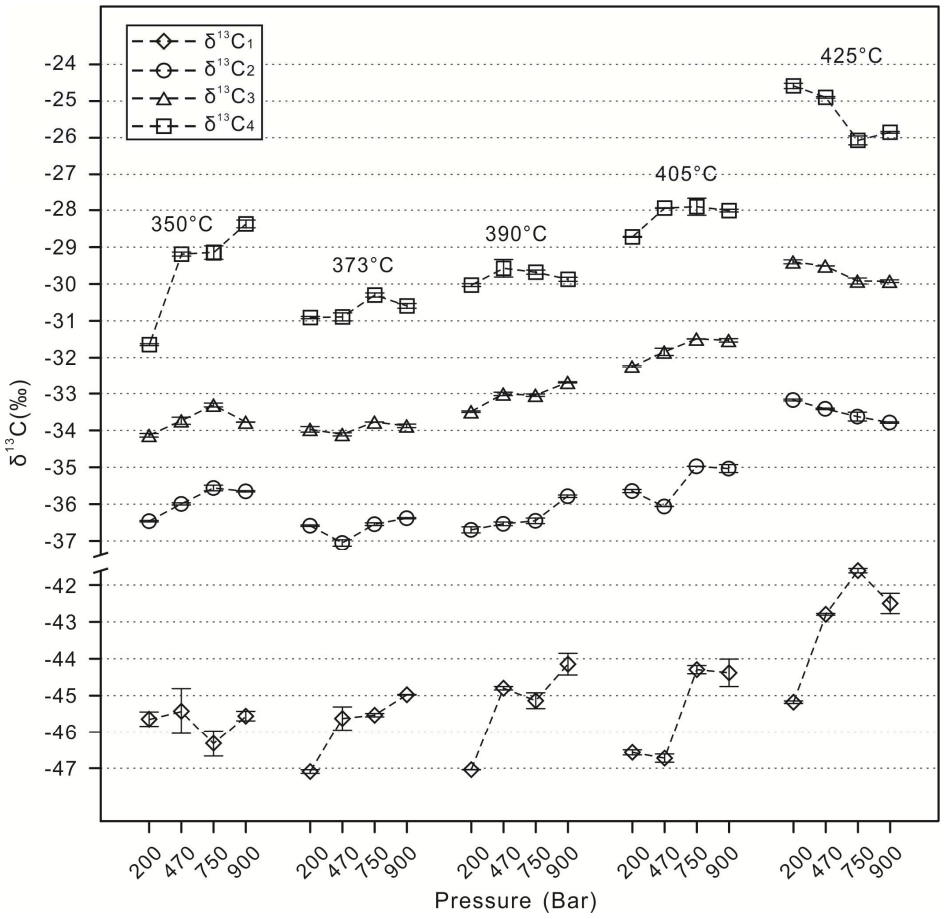

Figure 5. Carbon isotope ratios of individual hydrocarbon gas components with increasing pressure at different temperatures.

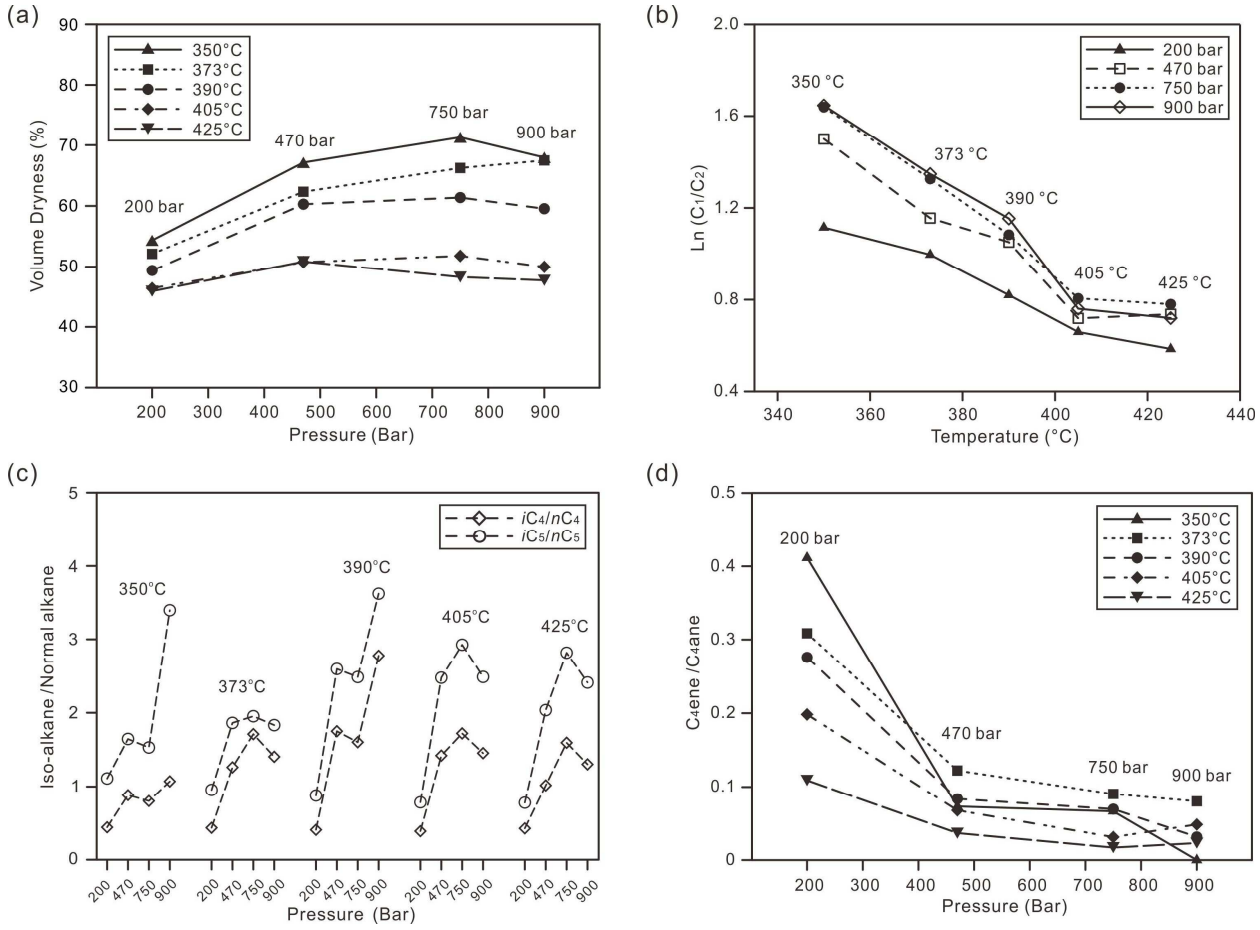

Figure 6. Changes in molecular parameters for hydrocarbon gases with increasing temperature and pressure. (a) dryness ($C_1/\Sigma C_{1-5}$ volume); (b) Ln(C_1/C_2 volume); (c) *iso*-/normal alkane; (d) butene/butane.

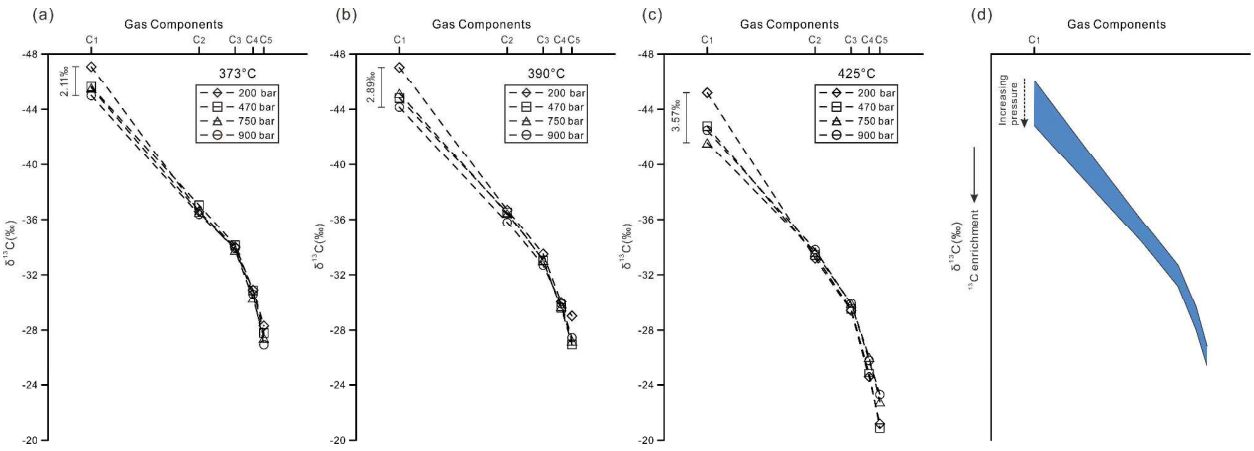

Figure 7. "Natural gas plot" of $\delta^{13}C(C_n)$ versus $1/C_n$ (after Chung *et al.*[37]). (a) 373 °C; (b) 390 °C; (c) 425 °C; (d) the overall conceptual model showing the effect of pressure.

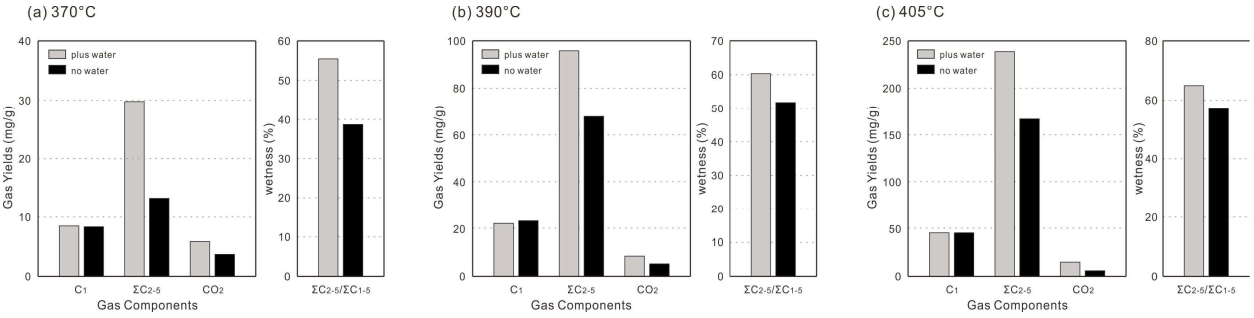

Figure 8. Gas yields (mg/g. oil) of individual gas components from the oil cracking experiments in gold capsules, in the presence and absence of water. (a) 370 °C; (b) 390 °C; (c) 425 °C.

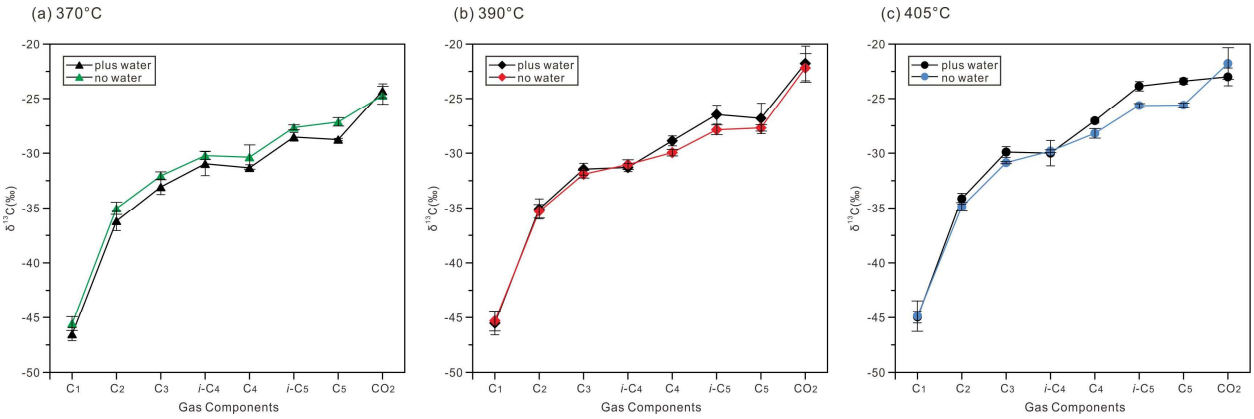

Figure 9. Stable carbon isotopic compositions of individual gas components from the oil cracking experiments in gold capsules, in the presence and absence of water. (a) 370 °C; (b) 390 °C; (c) 425 °C.